Research Article

Quinoline-Based Materials: Spectroscopic Investigations as well as DFT and TD-DFT Calculations

Mahmoud A. S. Sakr (ID),[1] **Samy A. El-Daly** (ID),[2] **El-Zeiny M. Ebeid** (ID),[1,2]
Sadeq M. Al-Hazmy (ID),[3,4] **and Mohammed Hassan** (ID)[5]

[1]*Misr University of Science and Technology (MUST), 6th October City, Egypt*
[2]*Chemistry Department, Faculty of Science, Tanta University, Tanta, Egypt*
[3]*Advance Diagnostic and Progressive Human Care Research Group, School of Biomedical Engineering and Health Science,*
 University Technology Malaysia, Johor Bahru, Malaysia
[4]*Chemistry Department, Faculty of Science, Qassim University, Qassim, Saudi Arabia*
[5]*Ibb University, Faculty of Science, Chemistry Department, Ibb, Yemen*

Correspondence should be addressed to Mohammed Hassan; m-hassan@ibbuniv.edu.ye

Quinoline derivatives such as 15,15-difluoro-[1,3,2] diaazaborininodiquinoline (DDP) and 15,15-difluoro-[1,3,2] diaazaborininodiquinoline acetonitrile (DDPA) have a range of biological and medical activities. So, it is vital to shed light on these compounds in terms of their optical properties supported by quantum calculations. The absorption and emission spectra of studied compounds were measured within the laboratory, whereas the quantum calculations were performed utilizing the density functional theory (DFT) calculations. Additionally, the time-dependent density functional theory (TD-DFT) was applied for the comparison of some sensible results with the theoretical ones. The molecular structures of these compounds were presented via applying chemical analysis techniques. The electronic absorption spectra of DDP and DDPA molecular structures were monitored through an experiment in hosts such as carbon tetrachloride (CCl_4), chloroform ($CHCl_3$), methylene dichloride (CH_2Cl_2), acetone, and dimethyl sulfoxide (DMSO). Also, the influence of pH on the absorption spectra of the DDP molecule was studied. The molecular structures of these quinoline derivatives have been optimized via utilizing the B3LYP/6-31G (d) level of theory. The electronic absorption and emission spectra of the DDP compound in gas, THF, and DMSO have been calculated utilizing TD-DFT at the CAM-B3LYP/6-31G ++(d, p) level.

1. Introduction

Quinoline is a heterocyclic compound with few chemical applications on its own. However, several of its derivatives have numerous applications such as pharmaceutical preparations [1], agricultural chemistry [2], materials and dyes [3], as well as in medicine. Recently, the nucleus of quinoline and plenty of its derivatives grasped interest to chemists and biologists owing to their many and necessary applications within the field of medicine as a number of them are used as antituberculosis [1, 4, 5], antimalarial [6], anticancer [7], antibiotic [8], hypotensive, antiviral [1], antioxidant [9], and

antifungal [10]. Given the wide importance of quinoline derivatives, it is absolutely necessary to shed light on them during this analysis.

Liquid quinoline dye lasers have significantly high potency, low optical device threshold, wide calibration varying from the near-ultraviolet to near-infrared spectral region, and long life [11, 12]. None of the opposite lasers will replace dye lasers for their strength, gain, low price, and big selection of viability [13]. However, these lasers cannot enter the industrialized market due to their inherent defects such as massive size, inflammable and cytotoxic solvents, dye deterioration, heating, and triplet state formation [14]. The dye

optical device resolution ought to flow through the optical device cavity to keep up stable gain and beam quality. This needs an outside variety of dye flow systems and reservoirs, and an outside quantity of dye is dissolved in typically inflammable and cytotoxic solvents [11–13, 15–17].

The electronic absorption spectra of DDP dye at completely different pH values show clear isosbestic points in their absorption spectra indicating the existence of two substances in equilibrium with each other [12, 18–21] showing an isosbestic point. However, the presence of associated degree isosbestic point is not a continuous proof of the existence of solely two compounds because the third absorbing species might have zero absorptivity at this specific wavelength [22].

The main objective of the study in this manuscript is the spectroscopic investigations and computational calculations of compounds under study using the DFT method followed by the determination of the accurate functional as well as the basis set using TD-DFT to arrive at the accurate theoretical results and comparing them with the experimental ones.

2. Materials and Methods

2.1. Materials' Preparation. 15,15-Difluoro-[1,3,2] dia-azaborininodiquinoline (DDP) and 15,15-difluoro-[1,3,2] diaazaborininodiquinoline acetonitrile (DDPA) were provided by Professor Dr. Ewald Daltrozzo of Konstanz University, Germany, and used without further purification. All solvents employed in this work were of chemical analysis grade and were preliminary checked for the absence of absorbing or fluorescent impurities among the scanned spectral ranges. UV-Vis electronic absorption spectra were obtained utilizing a Shimadzu UV-Vis 1650-PC spectrophotometer, and steady-state fluorescence spectra were presented employing a quartz cuvette of 0.2 cm path length to minimize the reabsorption of emitted photons; the emission was monitored at 90° geometry using a Jasco FP-8200 spectrofluorometer, excitation bandwidth 5 nm and emission bandwidth 5 nm, with a Xe lamp light source.

2.2. Methodology and Theoretical Calculations. Upon usage of density functional theory (DFT) and time-dependent density functional theory (TD-DFT) strategies, the ground electronic structure and excited state structures of the probe dye area unit were improved using the Gaussian 09 package [23]. The molecular structures under study have been optimized employing [24–26] the DFT/B3LYP/6-31G (d) level of theory. The electronic absorption and emission spectra of the quinoline derivatives in numerous solvents have been calculated exploiting the TD-DFT [27] at the CAM-B3LYP/6-31G ++(d, p) level.

3. Results and Discussion

3.1. DFT Calculations. The optimized molecular structures for DDP and DDPA molecules within the gaseous state area unit were obtained by the utilization of the B3LYP/6-31G (d) level of theory. The obtained results are shown in Figure 1. Some necessary calculated and optimized geometrical

parameters such as bond length (BL) in Å and bond angle (BA) and dihedral angle (DA) in degree (°) were computed for DDP and DDPA in gas at the ground (S_0) and initial excited state (S_1) using B3LYP/6-31G (d) level of theory; the obtained results are tabulated in Table 1. The labeling scheme for the studied molecular structures is shown in Figure 1. DFT was used to obtain the ground state (G) molecular structure of DDPA and DDP in the gaseous state. Also, TD-DFT was applied to obtain electronic excited state (Exc.) molecular modeling structures for DDP and DDPA in the gaseous phase. The optimized electronic ground and excited molecular structures were obtained via applying the B3LYB/6-31G (d) level of theory. As presented in Table 1 and Figure 1, the BLs (C_2-C_3 and C_1-C_{31}) for the DDPA compound and (C_3-C_4 and C_{13}-N_{32}) for DDP increase from G to Exc., and the difference values are 0.014 and 0.001 Å for DDPA and 0.021 and 0.006 Å for DDA. On the contrary, (C_2-N_{38} and N_{37}-C_{18}) BLs for DDPA and (C_3-N_{34} and N_{33}-C_{19}) BLs for DDA were shortened from S_0 to S_1 state. The difference values are 0.014 and 0.015 Å for DDPA and DDA, respectively. The DAs (C_{12}-C_7-C_2-C_{38}, C_{31}-C_{28}-N_{37}-C_{18}, C_{27}-C_{24}-C_{19}-C_{20} and B_{32}-N_{37}-C_{18}-C_{19}) for DDPA and (C_1-C_2-C_3-N_{34}, C_{19}-N_{33}-C_{28}-N_{32}, C_{29}-C_{25}-C_{18}-C_{17} and B_{31}-N_{33}-C_{19}-C_{18}) for DDP are 179.99° in the G and Exc. states. This is referring to the planar molecular structures for DDPA and DDP compounds in both G and Exc. states. The BAs (C_{11}-C_{12}-C_7, C_7-C_2-C_3 and N_{38}-B_{32}-N_{37}) for DDPA are increased via 0.04, 0.2, and 1.26, respectively, upon excitation from S_0 to S_1 state. On the contrary, the BAs (C_2-N_{38}-C_1 and N_{38}-C_1-C_{31}) for DDPA and (C_6-C_1-C_2, C_2-C_3-C_4, C_3-N_{34}-C_{13} and N_{34}-C_{13}-N_{32}) for DDP are shortened upon excitation from S_0 to S_1 state. The BAs for studied molecular structures in G and Exc. states indicate sp^2 hybridization.

The DDP and DDPA molecular modeling graphical presentation of the molecular orbitals HOMO (H)/LUMO (L), H − 1/L + 1, H − /L + together with their respective energy gaps (Egs) in the gaseous state were made via applying the B3LYP/6-31G (d) level of theory. The energy gaps go as follows: H and L (E_{g1}), H − 1 and L + 1 (E_{g2}), and H − 2 and L + 2 (E_{g3}) in the gaseous state via applying the B3LYP/6-31G (d) level of theory. The obtained results are presented in Figure 2. The energy values of H (E_H), L (E_L), H − 1 ($E_{H−1}$), L + 1 (E_{L+1}), H − 2 ($E_{H−2}$), and L + 2 (E_{L+2}) are presented in Figure 2. Also, the E_g values among the following, H and L (E_{g1}), H − 1 and L + 1 (E_{g2}), and H − 2 and L + 2 (E_{g3}), in the gaseous state are listed in Figure 2. Due to hyperconjugation of the studied molecular structures, the HOMO MOs and lone pairs of electrons of nitrogen and fluoride atoms are delocalized over the whole DDP and DDPA molecular structures. On the contrary, the LUMO MOs are delocalized over the whole DDP and DDPA molecular modeling structures, while the lone pairs of electrons of fluoride and nitrogen (N_{35} for DDPA and N_{32} for DDP) atoms are not contributed. The energy gap (E_{g1}) value is calculated by applying the difference ($E_L − E_H$). The calculated E_{g1} value for DDP and DPPA compounds increases in the order DDP < DDPA indicating that the DDP molecular modeling structure is more reactive compared to the DDPA molecular structure. When the magnitude of E_g increases, the kinetic
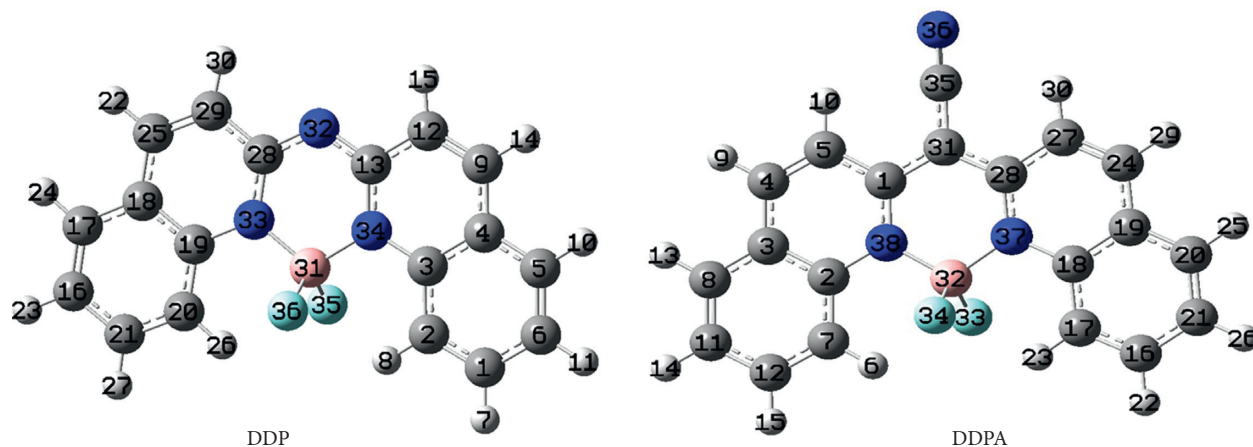
FIGURE 1: Optimized molecular structures for DDP and DDPA compounds in the gaseous state employing the B3LYP/6-31G (d) level of theory.

TABLE 1: Selected optimized geometrical parameters (bond length (BL) in Å and bond angle (BA) and dihedral angle (DA) in degree) computed for DDP and DDPA in the gaseous state at the ground (S_0) and initial excited state (S_1) employing the B3LYP/6-31G (d) level of theory. For labeling, refer to Figure 1.

Designation	DDPA		Designation	DDP	
	S_0	S_1		S_0	S_1
C_2-C_3	1.426	1.440	C_3-C_4	1.426	1.447
C_2-N_{38}	1.413	1.405	C_3-N_{34}	1.410	1.395
C_1-C_{31}	1.422	1.443	C_{13}-N_{32}	1.346	1.352
N_{37}-C_{18}	1.413	1.405	N_{33}-C_{19}	1.410	1.395
C_{11}-C_{12}-C_7	121.15	121.19	C_6-C_1-C_2	121.38	121.19
C_7-C_2-C_3	118.57	118.77	C_2-C_3-C_4	118.89	118.60
C_2-N_{38}-C_1	120.87	120.41	C_3-N_{34}-C_{13}	120.84	120.12
N_{38}-C_1-C_{31}	120.30	118.68	N_{34}-C_{13}-N_{32}	123.42	121.97
N_{38}-B_{32}-N_{37}	112.78	114.04	N_{34}-B_{31}-N_{33}	110.40	112.33
C_{12}-C_7-C_2-C_{38}	179.99	179.99	C_1-C_2-C_3-N_{34}	179.99	179.99
C_{31}-C_{28}-N_{37}-C_{18}	179.99	179.99	C_{19}-N_{33}-C_{28}-N_{32}	179.99	179.99
C_{27}-C_{24}-C_{19}-C_{20}	179.99	179.99	C_{29}-C_{25}-C_{18}-C_{17}	179.99	179.99
B_{32}-N_{37}-C_{18}-C_{19}	179.99	179.99	B_{31}-N_{33}-C_{19}-C_{18}	179.99	179.99

stability of the molecule increases, and chemical reactivity decreases [28]. Hence, the kinetic stability of the DDPA molecule is higher than DDP in the gaseous phase as shown in Figure 2.

Some significant quantum parameters such as dipole moment (μ), chemical potential (ρ), electronegativity (χ), and chemical hardness (η) were calculated from the energy values of Lumo (EL) and Homo (EH) molecular orbitals by applying the following equations: $\rho = (E_H + E_L)/2$ [23, 24], $\chi = -(E_H + E_L)/2$, and $\eta = (E_L - E_H)/2$ [23, 25]. Generally, once the chemical structure possesses high dipole moment, it acquires a large asymmetry in the electric charge distribution, and then it can be highly sensitive due to the change of molecular structure and electronic properties under an external electric field. Thus, as shown in Table 2, the μ value of the compound DDPA is high compared to the DDP compound; therefore, this compound is more active compared to the DDP molecular structure. As conferred in Table 2, the ρ value of the DDP molecular structure is lower compared to the opposite DDPA compound. This indicates that the escaping electrons from the DDP molecular

structure are low compared to the DDPA molecule. Also, the high χ value for the DDP molecular structure compared to the DDPA compound (see Table 2) results in the power of this compound to draw in electrons from different compounds [29]. On the contrary, the η value for the DDP molecular structure is high compared to DDPA (see Table 2). This means that the DDP compound is very difficult to liberate electrons, whereas the DDPA molecular structure is a good candidate to give electrons to another acceptor molecule.

3.2. Experimental UV-Vis Absorption Spectra. Experimental (Exp.) normalized absorption spectra (1×10^{-5} M) for DDP (Figure 3(a)) and DDPA (Figure 3(b)) in several solvents are obtained; the obtained results are shown in Figures 3(a) and 3(b). The Exp. maximum absorption wavelength λ_{abs} (Exp.) in several solvents for DDP and DDPA molecular structures' area unit is tabulated in Table 3. The two and three maximum absorption wavelengths of DDP and DDPA molecular structures were
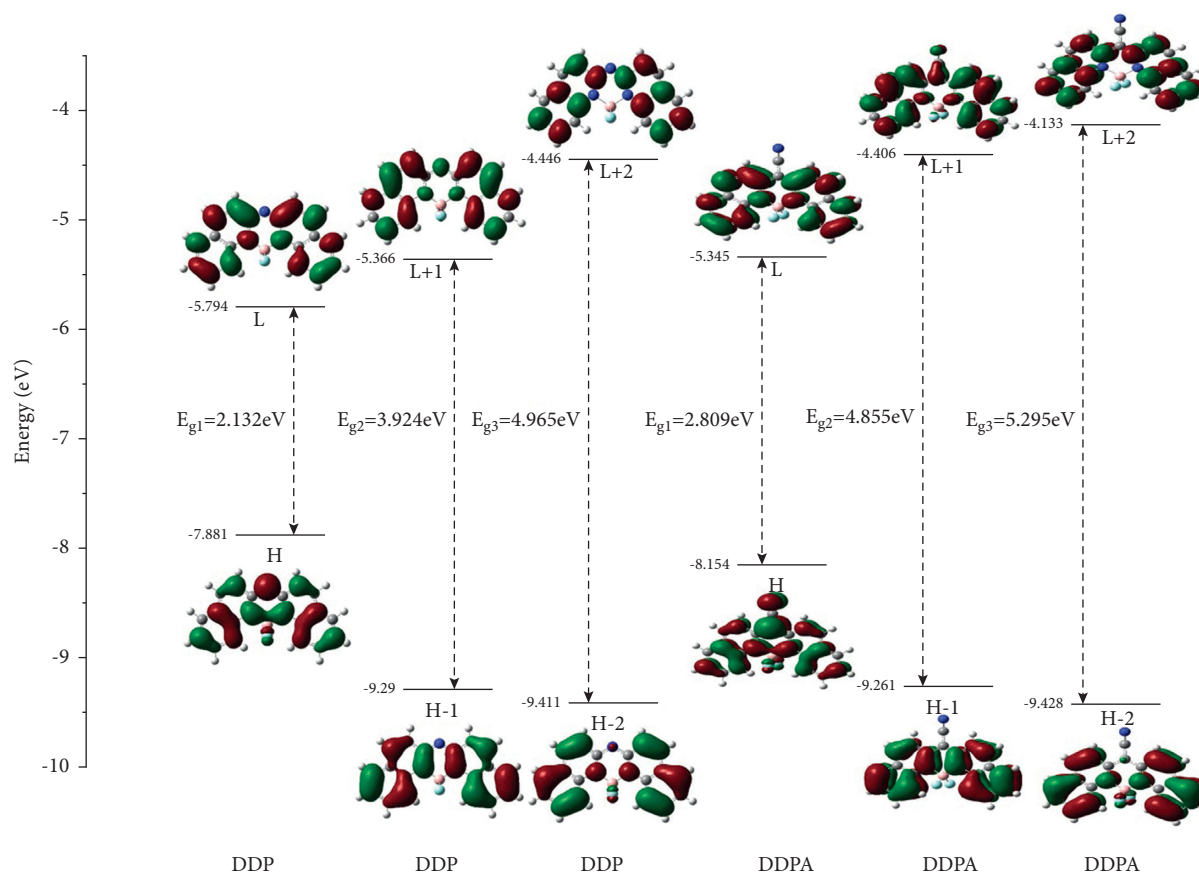
FIGURE 2: DDP and DDPA molecular modeling graphical presentation of HOMO (H)/LUMO (L) orbitals, $H-1/L+1$, and $H-2/L+2$ and the energy gap of H/L (E_{g1}), $H-1/L+1$ (E_{g2}), and $H-2/L+2$ (E_{g3}) in the gas state via utilizing the B3LYP/6-31G (d) level of theory.

TABLE 2: Calculated HOMO energy (E_H), LUMO energy (E_L), energy gap (E_{g1}), dipole moment (μ), and other quantum parameters such as electronegativity (χ), chemical potential (ρ), and chemical hardness (η) of DDP and DDPA molecular structures in the gaseous state obtained and obeying the B3LYP/6-31G (d) level of theory.

Compounds	E_H (eV)	E_L (eV)	E_{g1} (eV)	μ (D)	χ (eV)	ρ (eV)	η (eV)
DDPA	−8.154	−5.345	2.809	1.503	−6.749	6.749	1.404
DDP	−7.881	−5.749	2.132	2.153	−6.815	6.815	1.066

obtained by applying completely different solvents such as CCl_4, $CHCl_3$, CH_2Cl_2, acetone, and DMSO as presented in Figures 3(a) and 3(b) because of $\pi - \pi^*$ electronic transition and increasing electronic vibrations in the S_1 state. The values of maximum absorption wavelengths of DDP and DDPA molecular structures modified from one solvent to another are different because of solute/solvent interactions.

3.3. TD-DFT Calculations. Via applying the Gaussian 09 program, the best DFT functional of the DDP molecule is studied using the 6-31G (d) basis set. Also, the best basis set of the same molecule was investigated utilizing CAM-B3LYP DFT functional. Therefore, the best DFT functional and the basis set for calculating the optical properties of the DDP and DDPA molecules were CAM-B3LYP/6-311G++ (d, p). Upon utilizing the TD-DFT technique and CAM-B3LYP/6-311G++ (d, p) level of theory, the calculated UV-Vis absorption and emission spectra of the DDP molecule in different solvents

such as gaseous phase, THF, and DMSO are illustrated and compared with the obtained spectra recorded in Figure 4. The electronic calculated UV-Vis absorption spectrum of the DDP molecule in various solvents has three maximum absorption wavelengths (see Figure 4). The three maximum absorption wavelengths ($\lambda_{max.}$) of the DDP dye in the gaseous phase are 210, 265, and 391 nm. In the THF solvent, the three calculated $\lambda_{max.}$ values of the DDP molecule exist at 211, 265, and 398 nm. And in DMSO, the four λ_{max} absorption values are 183, 211, 265, and 398 nm matching the three and four maximum absorption wavelengths of the DDP molecular structure by applying gas, THF, and DMSO being of $\pi - \pi^*$ electronic transition at increasing electronic vibrational in the S_1 state. Depending on the polarity of solvents, the absorption maximum bands for the DDP molecule in THF and DMSO are redshifted compared to the gas state as shown in Figure 4.

For DDP dye in different solvents, the calculated electronic emission spectra have only one band of maximum emission wavelength ($\lambda_{max.}$) between 413 and 438 nm, depending on the
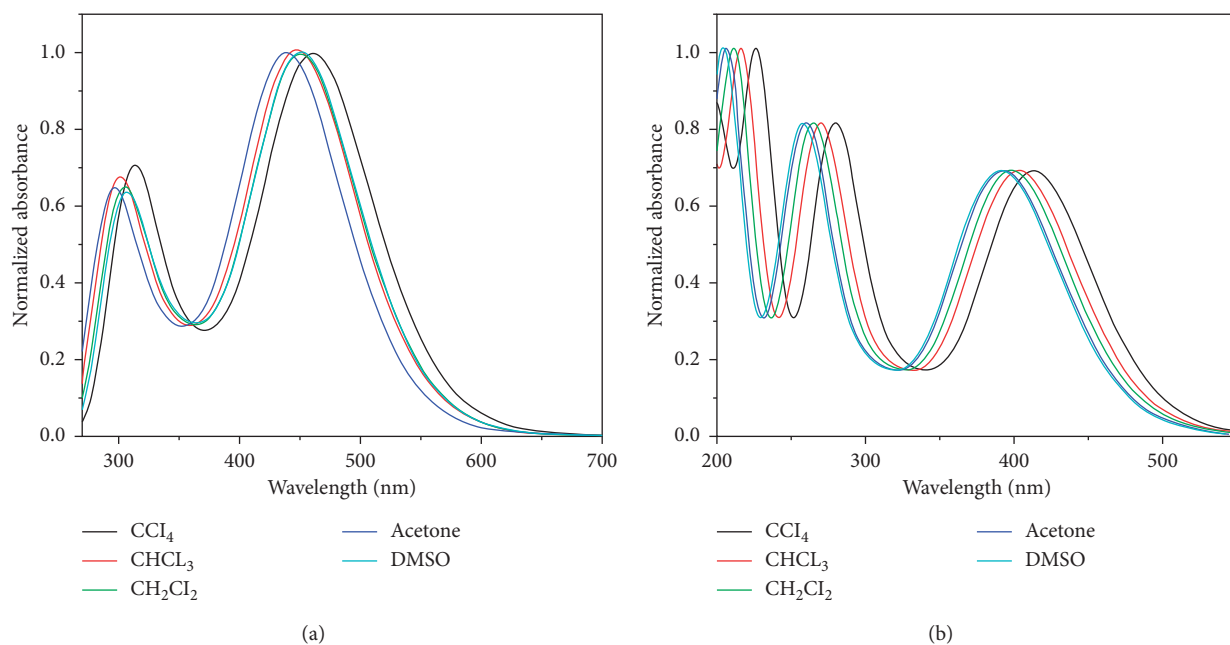
(a)

(b)

FIGURE 3: Experimental normalized absorption spectra (1×10^{-5} M) for DDP (a) and DDPA (b) in different solvents.

TABLE 3: Experimental maximum absorption wavelengths λ_{abs}(Exp.) in different solvents for DDP and DDPA molecular structures.

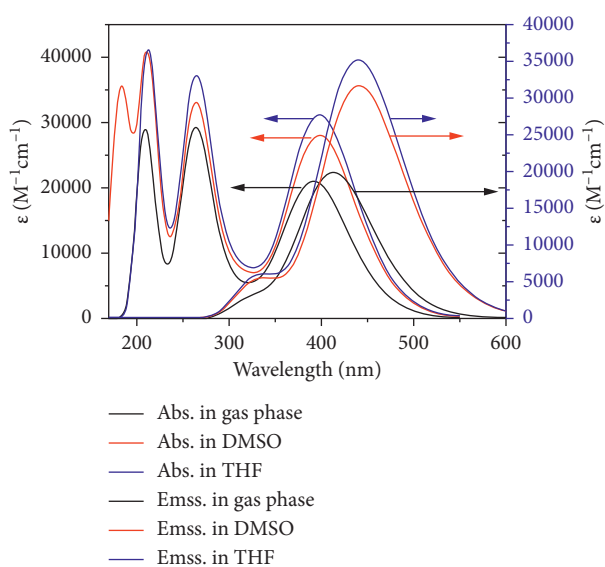| Solvents	λ_{abs} (Exp.) (nm) for DDP		λ_{abs} (Exp.) (nm) for DDPA		
CCl_4	313	462	226	280	413
$CHCl_3$	300	446	404	269	404
CH_2Cl_2	305	449	211	264	340
Acetone	295	440	206	260	395
DMSO	303	450	204	259	389

FIGURE 4: Calculated electronic absorption and emission spectra for the DDP molecule in the gaseous phase (in black), DMSO (in red), and THF (in blue). CAM-B3LYP/6-311G++ (d, p) was applied.

polarity of the solvents. Because of the high polarity of DMSO compared to THF and gas phase, the λ_{max} emission of the DDP molecule in DMSO is red-shifted (438 nm) compared to that in THF (437 nm) and gas phase (413 nm). Due to the overlap between calculated absorption and emission spectra of the DDP molecule, a part of photons from the emission spectrum of the DDP molecule is reabsorbed via the inner filter effect. As presented in Table 4, the calculated electronic absorption and emission spectra of the DDP molecule in numerous solvents via victimization CAM-B3LYP/6-311G++ (d, p) level of theory are in reasonable agreement with the experimental observation. The electronic transitions in THF were reconsidered according to previous data available to us. The calculated electronic absorption spectrum of DDP in THF is available at six possible electronic transitions at 398 ($f = 0.5143$), 330 ($f = 0.0219$), 314 ($f = 0.0448$), 310 ($f = 0.0354$), 265 ($f = 0.4749$), and 211 ($f = 0.5159$) nm. Accordingly, three of the new values agree with experimental results. This was quoted in Table 2 showing an agreement between theoretical and experimental results. The first, second, and third electronic transitions correspond to the experimental peaks at 398, 330, and 314 nm arising from HOMO $\longrightarrow$ LUMO, HOMO $\longrightarrow$ LUMO + 1, and HOMO − 1 $\longrightarrow$ LUMO transitions.

The optimal DFT functional and the basis set for calculating the optical properties of the DDPA molecule were CAM-B3LYP/6-311G++ (d, p). Hence, the calculated electronic UV-Vis absorption and emission spectra of the DDPA molecule in different solvents such as CCl_4, CH_3Cl, CH_2Cl_2, acetone, and DMSO were compared with the CAM-B3LYP/6-311G++(d, p) level of theory. The obtained spectra are shown in Figure 5. The UV-Vis absorption spectra have two maximum absorption wavelengths assigned to $\pi - \pi^*$ and $n - \pi^*$ as shown in Figure 5. Depending on the polarity of various solvents, the two maximum absorption wavelengths of DDPA are shifted to a longer wavelength (red-shifted) once the polarity of the

TABLE 4: Experimental (Exp.) and theoretical (Th.) maximum absorption (λ_{abs}) and emission ($\lambda_{emss.}$) wavelengths for the DDP molecule within DMSO and THF solvents. CAM-B3LYP/6-311G++ (d, p) was applied.

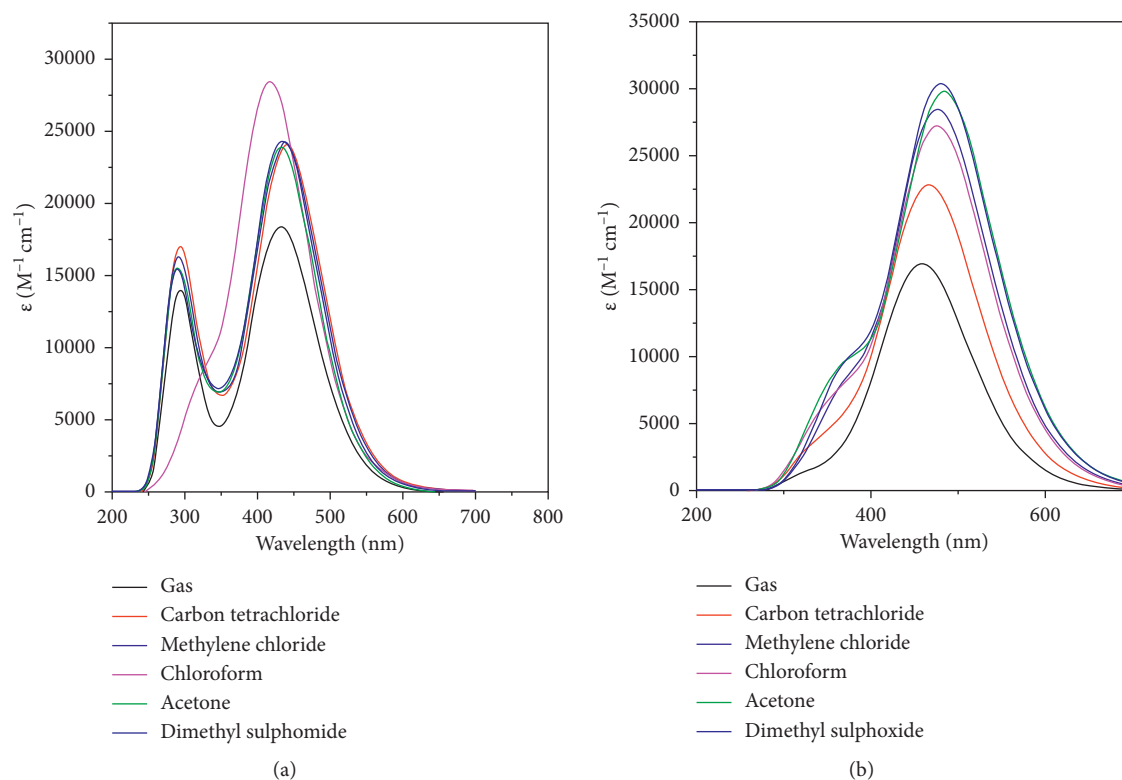| Solvents	λ_{abs} (Exp.) (nm)			λ_{abs} (Th.) (nm)			$\lambda_{emss.}$ (Exp.) (nm)	$\lambda_{emss.}$ (Th.) (nm)
DMSO	204	259	389	211	265	398	441	438
THF	334	365	424	314	330	398	439	437

FIGURE 5: Calculated absorbance (a) and emission (b) spectra of the DDPA molecule in different solvents. The CAM-B3LYP/6-311G++ (d, p) level of theory was applied.

solvents is decreased as shown in Figure 5 and Table 5. For the DDPA molecular structure in numerous solvents, the emission spectra show only one band of maximum emission wavelength ($\lambda_{max.}$) between 461 and 481 nm, depending on the polarity of the solvents. Owing to the high polarity of DMSO compared to alternative solvents and gaseous phase, the λ_{max} emission of the DDPA molecule in DMSO is red-shifted (482 nm) compared to other solvents and gaseous phase. Due to overlapping between calculated electronic absorption and emission spectra of the DDPA molecule, inner filter effect leads to reabsorption of photons from the short-wavelength component of the emission spectrum. By comparing the experimental results of DDPA (Table 3) with the theoretical results for the same compound (Table 5), we find that the theoretical results agree with the experimental ones. By the comparison the absorption spectrum of compounds under study, as its absorption spectrum ranges (300 to 500 nm) that match previously reported quinoline derivatives that have been studied in literature [30, 31] of showing absorbance in the range 280 to 510 nm. So, there is an agreement between the theoretical calculations in this manuscript and the other previous research studies. Hence, the

TABLE 5: Calculated maximum absorption (λ_{abs}) and emission wavelengths (λ_{ems}) of the DDPA molecule in different solvents.

Solvents	$\lambda_{abs.}$ (nm)		$\lambda_{ems.}$ (nm)
Gas	295	433	461
Carbon tetrachloride	294	442	469
Chloroform	291	438	478
Methylene chloride	—	436	479
Acetone	289	432	480
DMSO	287	431	482

CAM-B3LYP/6-311G++(d, p) level of theory is best for calculating UV-Vis absorption spectra of quinoline derivatives.

3.4. Molecular Electrostatic Potential (MESP) Maps. The molecular electrostatic potential (MESP) maps [27, 28] for DDP and DDPA molecular structures via applying the B3LYP/ 6-31G (d) [29, 32] level of theory are obtained. The graphical MESP maps are shown in Figure 6. At the surface of the studied molecular structure, the MESP is characterized via totally different colors as shown in Figure 6. In the MESP map, the red
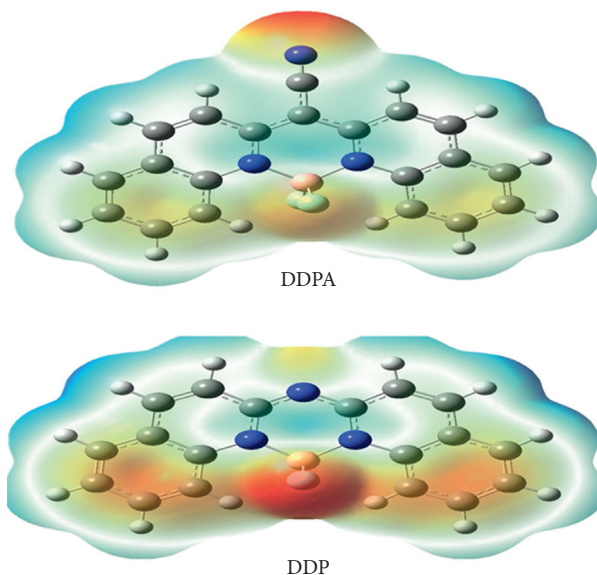
DDPA

DDP

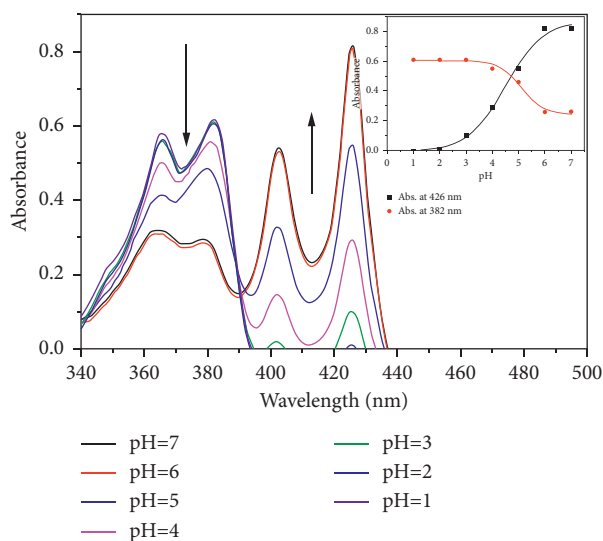FIGURE 6: MESP maps for DDP and DDPA molecular structures using the B3LYP/6-31G (d) level of theory.

FIGURE 7: The electronic absorption spectra of 1×10^{-5} M for DDP dye at several pH values. The inset shows the plot of absorbance of 1×10^{-5} M for DDP dye versus pH.

color regions correspond to negative MESP (electrophilic reactivity), the blue color sites refer to positive MESP (nucleophilic reactivity), and the green color parts relate to zero MESP. Therefore, the negative potential site in DDP is the BF_2 group, as well as the positive potential regions in the DDP molecule are around the hydrogen atoms as bestowed in Figure 6. On the contrary, the negative potential site in DDPA is the C = N cluster, as well as the positive potential regions within the same molecule are around the hydrogen atoms as bestowed in Figure 6.

3.5. Studying the Effect of pH on the DDP Molecule in Methanol.
It was noted during the study that the quinoline derivatives are affected by the acidic medium, so it was important to study the effect of the acidic medium on one of these compounds as an example to assess the extent of the effect of pH on the quinoline family. For the DDP molecule in methanol, the experimental electronic absorption spectra at different pH values are studied; the obtained spectra are shown in Figure 7. Due to protonation of (=N) within the DDP molecule utilizing the acidic medium, the maximum absorption bands at 366 and 382 nm are decreased. At the same time, the maximum absorption bands at 403 and 426 nm are increased. The isosbestic point of the DDP molecule occurs at 391 nm. According to the half-height technique and upon utilizing UV-spectrophotometric titration (Figure 7 inset), the ground-state protonation constant (pKa) was determined. From electronic absorption spectra of the DDP molecule, the magnitude of pKa is 4.72.
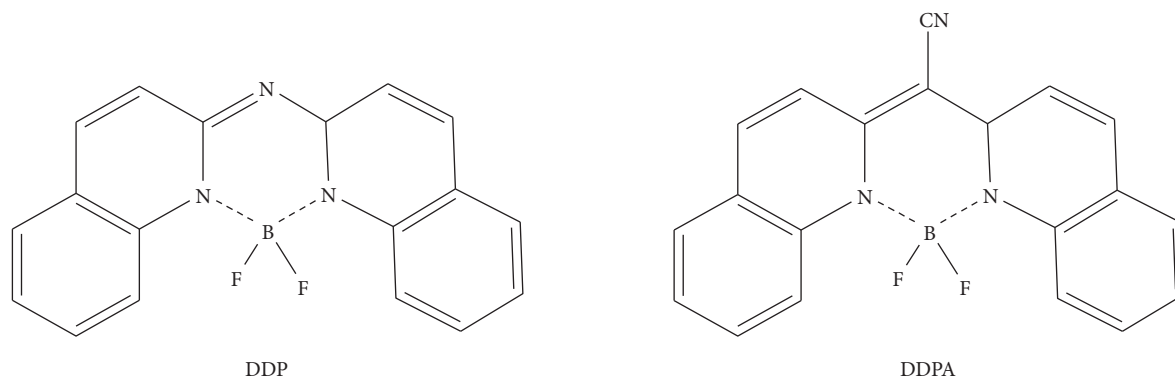
FIGURE 8: The molecular structures of DDP and DDPA.

The excited-state protonation constant (pKa^*) is calculated by using the following equation: $pK_a - pK_{a^*} = 2.1 \times^{-3} (\mathfrak{v}_{BH^+} - \mathfrak{v}_B)$, where ($\mathfrak{v}_{BH^+} - \mathfrak{v}_B$) refers to the difference between the wavenumbers (cm^{-1}) of the electronic transition of the pure acidic and conjugate base. The pKa^* value was found to be −0.95 indicating high basicity of the DDP molecule. Figure 8 shows the molecular structures of DDP and DDPA.

4. Conclusion

The molecular structures of the quinoline derivatives were optimized via applying the B3LYP/6-31G (d) level of theory. The electronic absorption and emission spectra of the DDP compound in gas, THF, and DMSO were calculated exploiting the time-dependent density functional theory (TD-DFT) at the CAM-B3LYP/6-31G ++(d, p) level. The calculated electronic absorption and emission spectra for DDP agree with experimental results. The experimental electronic absorption spectra for the DDP molecule in methanolic solutions of different pH values are studied. The molecular electrostatic potential (MESP) maps for DDP and DDPA molecular structures via applying the B3LYP/6-31G (d) level of theory are obtained.

Data Availability

The data used to support the findings of this study are available from the corresponding author upon request.

Conflicts of Interest

The authors declare no conflicts of interest.

References

[1] A. Lilienkampf, J. Mao, B. Wan, Y. Wang, S. G. Franzblau, and A. P. Kozikowski, "Structure–Activity relationships for a series of quinoline-based compounds active against replicating and nonreplicating Mycobacterium tuberculosis," *Journal of Medicinal Chemistry*, vol. 52, no. 7, pp. 2109–2118, 2009.

[2] S. Eswaran, A. V. Adhikari, I. H. Chowdhury, N. K. Pal, and K. D. Thomas, "New quinoline derivatives: synthesis and investigation of antibacterial and antituberculosis properties," *European Journal of Medicinal Chemistry*, vol. 45, no. 8, pp. 3374–3383, 2010.

[3] R. A. Mekheimer, M. A. Al-Sheikh, H. Y. Medrasi, and K. U. Sadek, "Advancements in the synthesis of fused tetracyclic quinoline derivatives," *RSC Advances*, vol. 10, no. 34, pp. 19867–19935, 2020.

[4] R. S. Keri and S. A. Patil, "Quinoline: a promising antitubercular target," *Biomedicine & Pharmacotherapy*, vol. 68, no. 8, pp. 1161–1175, 2014.

[5] Team R. C., ÐCengel, Y. A. B., ÐCengel, M. A. Y. A., Boles, M. A., ÐCengel, Y. A. C., ÐCengel, J. M. Y. A., & Cimbala J. M. (2012). T (No. 536. 7). M-H (2012). T (No. 536. 7). M-H, MILLS, Anthony F. Transferencia de calor. Irwin 1995., Payerle G. Scholar (4). Professional psychology;3:45.

[6] K. Kaur, M. Jain, R. P. Reddy, and R. Jain, "Quinolines and structurally related heterocycles as antimalarials," *European Journal of Medicinal Chemistry*, vol. 45, no. 8, pp. 3245–3264, 2010.

[7] S. Bongarzone and M. L. Bolognesi, "The concept of privileged structures in rational drug design: focus on acridine and quinoline scaffolds in neurodegenerative and protozoan diseases," *Expert Opinion on Drug Discovery*, vol. 6, no. 3, pp. 251–268, 2011.

[8] P. A. More and G. S. Shankarling, "Energy efficient Pfitzinger reaction: a novel strategy using a surfactant catalyst," *New Journal of Chemistry*, vol. 41, no. 21, pp. 12380–12383, 2017.

[9] A. L. Barry, "Procedure for testing antimicrobial agents in agar media: theoretical considerations," *Antibiotics in Laboratory Medicine*, pp. 1–26, Oxford Academic, Oxford, UK, 1986.

[10] A. Martin, M. Camacho, F. Portaels, and J. C. Palomino, "Resazurin microtiter assay plate testing of Mycobacterium tuberculosis susceptibilities to second-line drugs: rapid, simple, and inexpensive method," *Antimicrobial Agents and Chemotherapy*, vol. 47, no. 11, pp. 3616–3619, 2003.

[11] A. V. Deshpande, J. R. Rane, and L. V. Jathar, "Comparison of spectroscopic and lasing properties of different types of sol-gel glass matrices containing Rh-6G," *Journal of Fluorescence*, vol. 19, pp. 1083–93, 2009.

[12] C. Adamo and V. Barone, "Toward reliable density functional methods without adjustable parameters: the PBE0 model," *The Journal of Chemical Physics*, vol. 110, no. 13, pp. 6158–6170, 1999.

[13] A. V. Deshpande and U. Kumar, "Effect of method of preparation on photophysical properties of Rh-B impregnated sol-gel hosts," *Journal of Non-crystalline Solids*, vol. 306, no. 2, pp. 149–159, 2002.

[14] D. Avnir, D. Levy, and R. Reisfeld, "The nature of the silica cage as reflected by spectral changes and enhanced photo-stability of trapped rhodamine 6G," *Journal of Physical Chemistry*, vol. 88, no. 24, pp. 5956–5959, 1984.

[15] A. V. Deshpande and E. B. Namdas, "Efficient lasing action of rhodamine 6G in Nafion membranes," *Chemical Physics Letters*, vol. 263, no. 3-4, pp. 449–455, 1996.

[16] A. V. Deshpande and R. R. Panhalkar, "Spectroscopic properties of coumarin 2 in HCl and HNO_3 catalysed sol-gel glasses," *Journal of Luminescence*, vol. 96, no. 2–4, pp. 185–193, 2002.

[17] D. Avnir, V. R. Kaufman, and R. Reisfeld, "Organic fluorescent dyes trapped in silica and silica-titania thin films by the sol-gel method. Photophysical, film and cage properties," *Journal of Non-crystalline Solids*, vol. 74, no. 2-3, pp. 395–406, 1985.

[18] S. Tavker, P. Kumar P, H. R. Carlon, and M. E. Milham, "Isosbestic point: an application for aerosol spectrometry," *Journal of Geophysical Research: Atmospheres*, vol. 102, no. D25, pp. 30017–30022, 1997.

[19] M. J. van Staaden, H. Römer, and V. C. K. Couldridge, "1 A novel approach to hearing: the acoustic world of pneumorid. Complex worlds from simpler," *Nervous System*, vol. 335, 2004.

[20] H. R. Carlon, "Practical upper limits of the optical extinction coefficients of aerosols," *Applied Optics*, vol. 18, no. 9, pp. 1372–1375, 1979.

[21] H. R. Carlon, "Isosbestics in infrared aerosol spectra: proposed applications for remote sensing," *Infrared Physics*, vol. 21, no. 2, pp. 93–99, 1981.

[22] P. Chýlek, G. Videen, D. Ngo, R. G. Pinnick, and J. D. Klett, "Effect of black carbon on the optical properties and climate forcing of sulfate aerosols," *Journal of Geophysical Research: Atmospheres*, vol. 100, pp. 16325–16332, 1995.

[23] Frisch M., Trucks G. W., Schlegel H. B., Scuseria G. E., Robb M. A., Cheeseman J. R., et al. Gaussian~09 revision D. 01 2014.

[24] B. Miehlich, A. Savin, H. Stoll, and H. Preuss, "Results obtained with the correlation energy density functionals of Becke and Lee, Yang and Parr," *Chemical Physics Letters*, vol. 157, no. 3, pp. 200–206, 1989.

[25] S. U. Lee, "Influence of exchange-correlation functional in the calculations of vertical excitation energies of halogenated copper phthalocyanines using time-dependent density functional theory (TD-DFT)," *Bulletin of the Korean Chemical Society*, vol. 34, no. 8, pp. 2276–2280, 2013.

[26] J. Sun, G. Li, and W. Liang, "How does the plasmonic enhancement of molecular absorption depend on the energy gap between molecular excitation and plasmon modes: a mixed TDDFT/FDTD investigation," *Physical Chemistry Chemical Physics*, vol. 17, no. 26, pp. 16835–16845, 2015.

[27] E. Katchalski-Katzir, E. Haas, and I. Z. Steinberg, "Study of conformation and intramolecular motility of polypeptides in solution by a novel fluorescence method," *Annals of the New York Academy of Sciences*, vol. 366, pp. 44–61, 1981.

[28] S. A. Abdel-Latif and A. A. Mohamed, "Synthesis, spectroscopic characterization, first order nonlinear optical properties and DFT calculations of novel Mn(II), Co(II), Ni(II), Cu(II) and Zn(II) complexes with 1,3-diphenyl-4-phenylazo-5-pyrazolone ligand," *Journal of Molecular Structure*, vol. 1153, pp. 248–261, 2018.

[29] S. A. El-Daly and K. A. Alamry, "Spectroscopic investigation and photophysics of a D-π-A-π-D type styryl pyrazine derivative," *Journal of Fluorescence*, vol. 26, no. 1, pp. 163–176, 2016.

[30] M. Khalid, M. A. Ullah, M. Adeel, M. Usman Khan, M. N. Tahir, and A. A. C. Braga, "Synthesis, crystal structure analysis, spectral IR, UV-Vis, NMR assessments, electronic and nonlinear optical properties of potent quinoline based derivatives: interplay of experimental and DFT study," *Journal of Saudi Chemical Society*, vol. 23, no. 5, pp. 546–560, 2019.

[31] G. C. Dos Santos, R. O. Servilha, E. F. de Oliveira, F. C. Lavarda, V. F. Ximenes, and L. C. da Silva-Filho, "Theoretical-experimental photophysical investigations of the solvent effect on the properties of green- and blue-light-emitting quinoline derivatives," *Journal of Fluorescence*, vol. 27, no. 5, pp. 1709–1720, 2017.

[32] M. Bourass, A. T. Benjelloun, M. Benzakour et al., "DFT and TD-DFT calculation of new thienopyrazine-based small molecules for organic solar cells," *Chemistry Central Journal*, vol. 10, pp. 67–11, 2016.